Mercury distribution and transport in the North Atlantic Ocean along the GEOTRACES-GA01 transect

Daniel Cossa[1], Lars-Eric Heimbürger[2], Fiz F. Pérez[3], Maribel I. García-Ibáñez[4,3], Jeroen E. Sonke[5], Hélène Planquette[6], Pascale Lherminier[7], Julia Boutorh[6], Marie Cheize[6], Jan Lucas Menzel Barraqueta[8], Rachel Shelley[6], and Géraldine Sarthou[6]

[1]*ISTerre, Université Grenoble Alpes, CS 40700, F-38058 Grenoble Cedex 9, France*
[2]*Aix Marseille Université, CNRS/INSU, Université de Toulon, IRD, Mediterranean Institute of Oceanography (MIO) UM 110, Marseille, France*
[3]*Instituto de Investigaciones Marinas, CSIC, Eduardo Cabello 6, E-36208 Vigo, Spain*
[4]*Uni Research Climate, Bjerknes Centre for Climate Research, Bergen 5008, Norway*
[5]*CNRS, GET-OMP, 14 Ave. E. Belin, F-31240 Toulouse, France*
[6]*LEMAR, Université de Bretagne Occidentale, F-29280 Plouzané, France*
[7]*IFREMER, Brittany Center, LPO, BP 70, F-29280 Plouzané, France*
[8]*GEOMAR, Helmholtz Centre for Ocean Research, D-24148 Kiel, Germany*

Abstract

We report here the results of total mercury (HgT) determinations along the 2014 GEOTRACES GEOVIDE cruise (GA01 transect) in the North Atlantic Ocean (NA) from Lisbon (Portugal) to the Labrador coast (Canada). HgT concentrations in unfiltered samples (HgT_{UNF}) were log-normally distributed and ranged between 0.16 and 1.54 pmol L^{-1}, with a geometric mean of 0.51 pmol L^{-1} for the 535 samples analysed. The dissolved fraction (< 0.45 µm) of HgT (HgT_F), determined on 141 samples, averaged 78 % of the HgT_{UNF} for the entire data set, and 84 % for open sea waters (below 100 m) and 91 % if the Labrador Sea data, where the primary production was high (with a winter convection down to 1400 m), are excluded. HgT_{UNF} concentrations increased eastwards and with depth from Greenland to Europe and from sub-surface to bottom waters. The HgT_{UNF} concentrations were similarly low in the Subpolar Gyre waters (~ 0.45 pmol L^{-1}), whereas they exceeded 0.60 pmol L^{-1} in the Subtropical Gyre waters. The HgT_{UNF} distribution mirrored that of dissolved oxygen concentration, with highest

concentrations levels associated with oxygen-depleted zones. The relationship between HgT_F and the apparent oxygen utilization confirms the nutrient-like behavior of Hg in the NA. An extended Optimum Multiparameter Analysis allowed us to characterize HgT_{UNF} concentrations in the different Source Water Types (SWTs) present along the transect. The distribution pattern of HgT_{UNF}, modeled by mixing of SWTs, show Hg-enrichments in Mediterranean Waters and North East Atlantic Deep Water, and low concentrations in young waters formed in the Subpolar Gyre and Nordic seas. The change in anthropogenic Hg concentrations in the Labrador Sea Water, during its eastward journey, suggests a continuous decrease of Hg content in this water mass over the last decades. Calculation of the water transport driven by the Atlantic Meridional Overturning Circulation across the Portugal-Greenland transect indicates a northward Hg transport within the upper limb, and a southward Hg transport within the lower limb, with a resulting net northward transport of about 97.2 kmol yr^{-1}.

1. Introduction

The ocean plays a central role in the global mercury (Hg) cycle. It receives Hg mainly from atmospheric deposition, whereas it disposes of it in deep marine sediments (e.g., Mason et al., 1994). In the meantime, the largest part of Hg is recycled in the atmosphere, while a smaller fraction penetrates the ocean interior *via* thermohaline circulation or the biological pump (see reviews by Mason and Sheu, 2002; Fitzgerald et al., 2007 and Mason et al., 2012). Firstly, Hg reinjection to the atmosphere results from the formation of volatile elemental Hg *via* photoreduction and microbiological reduction of divalent Hg (e.g., Mason et al., 1995; Amyot et al., 1997). Secondly, the Hg

integration into thermohaline circulation involves its solubilization in surface waters followed by the subduction of these water masses along isopycnals (e.g., Gill and Fitzgerald, 1988). Thirdly, the biological pump consists of Hg sorption onto biogenic particles produced in the euphotic zone, then its conveying at depth by sinking materials, with a possible Hg remobilization, due to the particulate remineralization-dissolution process (e.g., Mason et al., 1993). The shape of observed vertical oceanic Hg profiles, characterized by increasing concentrations with depth, includes the marks of these different routes and is akin to "nutrient-type" profiles (Gill and Fitzgerald, 1988; Cossa et al., 2004; Lamborg et al., 2014; Bowman et al., 2015, 2016). The Hg cycle is also known as being highly perturbed by human activities (e.g., Mason et al., 2012; Lamborg et al., 2014; Zhang et al., 2014; Amos et al., 2015). Modern Hg concentrations in the global atmosphere are more than three times the pre-industrial Hg concentrations, leading to increasing of the Hg concentrations in surface and intermediate oceanic layers, which remains to be precisely estimated. Albeit these advances in the knowledge of the Hg biogeochemical cycle, the key features of the Hg distribution among the principal oceanic water masses are still poorly documented. Recent enhancements in precision and accuracy of Hg analyses allow more reliable vertical Hg profiles in the water columns (e.g., Cossa et al., 2011; Lamborg et al., 2014; Heimbürger et al., 2015; Bowman et al., 2015, 2016; Munson et al., 2015; Cossa et al., 2017a and b). In addition, an original approach for the estimation of the anthropogenic fractions of Hg concentrations in oceanic waters has been proposed (Lamborg et al., 2014). Owing to these last methodological breakthroughs, significant advances in detailed Hg oceanic distributions are possible.

The North Atlantic Ocean (NA) plays an active role in the cycling of chemical species in the ocean because it is a region where deep water formation drives the Atlantic Meridional Overturning Circulation (AMOC) (Kuhlbrodt et al., 2007). Particularly in the subpolar NA, chemical properties, including Hg, are transported to the ocean interior; thus, NA offers a unique opportunity for studying the oceanic response to changes in atmospheric Hg deposition. The GEOTRACES-GA03 zonal and meridional transects, sampled in 2010 and 2011, covered the NA from East to West between 18°N and 40°N, from Africa to USA coasts. Here, we report the results of the GEOVIDE cruise, along the GEOTRACES-GA01 transect, which targeted the NA from 40°N to 60°N, from Portugal to Newfoundland, *via* the southern tip of Greenland (Fig. 1). This article provides (i) a high-resolution description of the HgT distribution in the waters of Subpolar and Subtropical gyres of the NA, (ii) a characterization the HgT concentrations of the main water masses of the NA, (iii) an estimate of the temporal change of anthropogenic Hg in LSW, and (iv) a quantification the HgT transport associated with the upper and lower limbs of the AMOC. These new data contribute a refinement of the depiction of the Hg distribution in the NA waters and should allow further improvements in the oceanic Hg modeling.

2. Oceanographic context

A full description of the water masses along the GEOTRACES-GA01 transect can be found in García-Ibáñez et al. (this issue). Briefly, the North Atlantic Current (NAC) conveys the warm salty surface waters from subtropical regions northwards to the subpolar regions, where they are cooled down by heat exchange with the atmosphere

(Fig. 1). The intermediate and deep waters formed this way fill up the Global Ocean, initiating the southward-flowing limb of the AMOC (e.g., McCartney and Talley, 1984; Lherminier et al., 2010). In addition, the general circulation pattern is characterized by the subtropical and the subpolar gyres (Fig. 1).

In the Subtropical Gyre (Fig. 1), several water masses can be identified. Listing them from top to bottom: (i) the mixed layer, (ii) the East North Atlantic Central Water (ENACW), (iii) the Mediterranean Water (MW), (iv) the Labrador Sea Water (LSW) and (v) the lower North East Atlantic Deep Water ($NEADW_L$), which contains about 30% Antarctic Bottom Water (AABW) (García-Ibáñez et al., 2015). The transformation of ENACW leads to the formation of different mode waters including the Subpolar Mode Waters (SPMWs) (McCartney and Talley, 1982; Tsuchiya et al., 1992; van Aken and Becker, 1996; Brambilla and Talley, 2008; Cianca et al., 2009). SPMWs are the near-surface water masses of the Subpolar Gyre of the NA characterized by thick layers of nearly uniform temperature, often notated with a temperature as a subscript ($SPMW_8$ for example). SPMWs are formed during winter convection at high latitude, due to atmospheric freshening of surface waters originating from the Subtropical Gyre (McCartney, 1992). SPMWs participate in the upper limb of the AMOC and provide much of the water that is eventually transformed into the several components of North Atlantic Deep Water (NADW; Brambilla and Talley, 2008).

In the Subpolar Gyre, ocean-atmosphere interaction is particularly intense. The cooling down of subtropical waters produces dense waters, triggering the deepening of the mixed layer and further leading to deep convection. The main NA convection zones are located in the Labrador (LS), Irminger (IrS) and Nordic seas (NS) (Fig. 1).

Convection in those zones leads to the formation of intermediate and deep waters such as LSW, Denmark Strait Overflow Water (DSOW) and Iceland-Scotland Overflow Water (ISOW). LSW and ISOW are the main components of NEADW, and the all three are the components of the NADW, which constitutes the cold deep southward-flowing limb of the AMOC, flowing towards the Southern Ocean in the western Atlantic basin. LSW has been variably produced in the past fifty years depending on the intensity of winter convection, linked to the intensity of the North Atlantic Oscillation (e.g., Rhein et al., 2002; Cianca et al., 2009; Yashayaev and Loder, 2016). Depths of winter convection in the LS vary from a few hundred meters (the early 2000s) to over 2000 m (early 1990s). The LSW is a thick layer in the LS and thins out as it travels southwestwardly. It spreads out into the entire NA, filling the Subpolar Gyre and entering the Subtropical Gyre. Within the Subpolar Gyre, LSW is marked by a salinity minimum above the ISOW. In both gyres, the well-ventilated LSW is noticeable by a marked oxygen maximum.

3. Material and methods

3.1. Sampling

Water samples were collected during the French-led GEOVIDE cruise (GEOTRACES-GA01 transect), on board the RV *Pourquoi Pas?* sailing from Lisbon (Portugal) on May 15th to arrive on June the 30th 2014 in St John's (Newfoundland, Canada) (Fig. 1). Seventy-eight (78) stations (Table S1) were occupied for hydrographic profiles (CTD, dissolved oxygen, nutrients), among which 29 included trace metal sampling. Sampling and water treatment for HgT determination (Lamborg et al., 2012; Cutter et al., 2017)

were performed using ultra-trace techniques following the GEOTRACES recommendations. During the GEOVIDE cruise, an epoxy-coated aluminum rosette, equipped with 12 L GO-FLO (General Oceanics®) bottles initially cleaned following the GEOTRACES procedures (Cutter and Bruland, 2012), was deployed on a 6 mm Kevlar hydrowire. The rosette was also equipped with probes for pressure, conductivity, temperature, dissolved oxygen, fluorometry and transmission measurements (titanium SBE model 911-plus, Sea-Bird Electronics®). Specifically, for Hg determination, all material in contact with the seawater samples was made of Teflon or Teflon coated, acid cleaned and rinsed with ultrapure water (Milli-Q, Millipore®) prior to utilization. Original vent fixture and sampling valves of the GO-FLO bottles were replaced with Teflon (PTFE) ones. GO-FLO bottles were sub-sampled under a laminar flow bench inside a trace metal clean container. The efficiency of the High-Efficiency Particulate Air filter (HEPA, 0.3 µm) in the container was checked with a Coulter Counter during the cruise. All subsequent sample treatments (including filtration) and Hg analyses were also performed in class 100 clean containers. For sample filtrations, acid-washed 0.45 µm polycarbonate membranes (Nuclepore) were preferred to cellulose acetate or polyethersulfone membranes proposed in the GEOTRACES protocols (Fig. S1). Sub-samples were stored in Teflon bottles (FEP) until the onboard HgT analyses, which occurred within 6 hours after sampling.

3.2. Chemical analyses

In order to access all Hg species, the release of Hg from its ligands was achieved by a BrCl solution (50 µL of a 0.2 N solution is added to a 40-mL sample), and then the Hg was reduced with an acidic $SnCl_2$ solution (100 µL of a 1 M solution is added to a 40-

mL sample). Potassium bromide (Sigma Aldrich, USA) and potassium bromate (Sigma Aldrich, USA) were heated for 4 h at 250°C to remove Hg traces before making up BrCl solution with freshly double-distilled HCl (Heimbürger et al., 2015). The generated Hg vapor was amalgamated into a gold trap and then released by heating into an atomic fluorescence spectrometer (AFS). We used two AFS systems in parallel (Tekran® Model 2500, Brooks® Model 3), both calibrated against the NIST 3133 certified reference material. This technique, initially described by Bloom and Crecelius (1983) and subsequently improved by Gill and Fitzgerald (1985), is now an authoritative procedure officialised by the US-EPA as method 1631 (EPA, 2002). The definitions of detection limit (DL), reproducibility and accuracy given here are adopted from Taylor (1987) and Hewitt (1989). Using a mirrored quartz cuvette (Hellma®) allowed for an "absolute DL", defined as two times the electronic noise magnitude, as low as 1.7 femtomoles. However, in practice for trace measurements, the DL is governed by the reproducibility of the blank values, and calculated as 3.3 times the standard deviation of blank values. The blank was determined on a purged Hg-free seawater sample spiked with reagents (i.e., BrCl and $SnCl_2$). The mean (± standard deviation) of blanks measured during the GEOVIDE cruise was 3.2 ± 1.0 femtomoles. Thus, for a 40-mL seawater aliquot, the DL expressed in HgT concentration was 0.07 pmol L^{-1}. The reproducibility (coefficient of variation of six replicate measures) varied according to the concentration level between 5 and 15 %. The accuracy of HgT measurements was tested using ORMS-5 certified reference material (CRM) from the National Research Council of Canada (http://www.nrc-cnrc.gc.ca/), as spike addition to a purged Hg-free seawater sample. Measurements were always within the given

confidence interval. To ensure good data quality, and as a continuity of previous efforts (Cossa and Courau, 1990; Lamborg et al., 2012), we organized the 2014 GEOTRACES intercalibration exercise for total HgT and methyl Hg as a part of the GEOVIDE cruise. The intercalibration sample was taken on June 22^{nd,} 2014 in the LS at 49.093°W, 55.842°N, and 2365 m-depth. The sample was sent out to 10 participating laboratories. This station was also planned as crossover station within the 2015 Arctic GEOTRACES effort (Canadian cruise) but has been changed subsequently to another location. Our results compare well with the consensus values, HgT = 0.63 ± 0.12 pmol L^{-1}, n = 8. We measured the 2014 GEOTRACES intercalibration sample twice for HgT and obtained 0.51 (22nd June 2014, on board) and 0.58 pmol L^{-1} (30th October 2014, home lab).

3.3. Extended Optimum Multiparameter analysis

We used an extended Optimum Multiparameter (eOMP) analysis to characterize the water mass HgT_{UNF} concentrations along the GEOTRACES-GA01 transect (García-Ibáñez et al., 2015, this issue). The eOMP analysis quantifies the proportions of the different Source Water Types (SWTs) that contribute to a given water sample. The HgT_{UNF} concentration of each SWT, $[HgT_{UNF}]_i$, was estimated through an inversion of the SWT fractions given by the eOMP analysis. Such an approach was successfully applied to dissolved-organic-carbon water mass definitions in the NA (Fontela et al., 2016) and for evaluating the impact of water mass mixing and remineralization on the N_2O distribution in the NA (de la Paz et al., 2017). Here, we performed an inversion of a system of 430 equations (HgT_{UNF} samples) and 11 unknowns ($[HgT_{UNF}]_i$). Samples for which the difference between the observed HgT_{UNF} and the predicted HgT_{UNF} values by the multiple linear regression (Eq. 1 below) was three times greater than the standard

deviation were removed from the analysis. Nine samples were concerned: Sta. 2 (125 m), Sta. 11 (793 m), Sta. 11 (5242 m), Sta. 13 (1186 m), Sta. 15 (170 m), Sta. 19 (99 m), Sta. 26 (97 m), Sta. 32 (596 m), and Sta. 38 (297 m). The SWTs were characterized by potential temperature, salinity, and macronutrients. The eOMP was restricted to depths below 75 m in order to avoid air-sea interaction effects. The eOMP gave us the fractions of the 11 SWTs, and we resolved the following expression to estimate the $[HgT_{UNF}]_i$:

$$[HgT_{\mathrm{UNF}}]_j = \sum_{i=1}^{11} SWT_i^j * [HgT_{\mathrm{UNF}}]_i + \varepsilon_j \quad (j = 1 \ldots 430) \quad (1)$$

where $[HgT_{UNF}]_j$ represents the measured HgT_{UNF} concentration for each sample *"j"*, SWT_i^j the proportion of SWT *"i"* to sample *"j"* (obtained through the eOMP), $[HgT_{UNF}]_i$ the HgT_{UNF} concentration for each SWT *"i"* (unknow), and ε_j the residual.

The 430 ε_js of the inversion presented a null mean and a standard deviation of 0.085 pmol L^{-1} (R = 0.84).

3.4. Mercury transport calculation

Velocity fields across the GEOTRACES-GA01 transect were calculated using inverse model constrained by Doppler current profiler velocity measurements (Zunino et al., this issue) an overall mass balance of 1 ± 3 Sv to the North (Lherminier et al., 2007, 2010). The volume transport per SWT was computed by combining these velocity fields with the results of the eOMP (García-Ibáñez et al., this issue). Finally, the HgT_{UNF} transports per water mass were calculated through Eq. (2):

$$T_{HgT_{\mathrm{UNF}}} = \sum_{i=1}^{11} T_{SWT_i} * [HgT_{\mathrm{UNF}}]_i * \rho_i \quad (2)$$

where T_{SWTi} is the volume transport of SWT "*i*", $[HgT_{UNF}]_i$ is the HgT_{UNF} concentration for each SWT *"i"* (from Eq. 1), and ρ_i is the density of the SWT *"i"*.

The inverse model configuration for the GEOVIDE cruise data is described in Zunino et al. (this issue). The inverse model is based on the least-squares formalism, which provides errors on the velocities and associated quantities such as the magnitude of the AMOC (estimated in density coordinate) and the heat flux (Lherminier et al., 2010). The inverse model computes the absolute geostrophic transports orthogonal to the section. The Ekman transport is deduced from the wind fields averaged over the cruise period and added homogeneously in the upper 40 m (Mercier et al., 2015). The transport estimates of the inverse model across the section have been validated by favorable comparisons with independent measurements (Gourcuff et al., 2011; Daniault et al., 2011; Mercier et al., 2015).

4. Results

Distributions of potential temperature, salinity, dissolved oxygen and silicic acid are given in García-Ibáñez et al. (this issue), and reproduced on figure S2.

HgT_{UNF} concentrations along the GEOTRACES-GA01 transect ranged from 0.16 to 1.54 pmol L^{-1} (n = 535), these data being log-normally distributed, positively skewed (Skewness = 1.1; Kurtosis = 2.1; Fig. S3) and with 97 % of the values lower than 1.00 pmol L^{-1}. The geometric mean and the median were 0.51 pmol L^{-1}, whereas the arithmetic mean and standard deviation were 0.54 and 0.19 pmol L^{-1}, respectively. These concentrations are within the range found along the GEOTRACES-GA03 transect

(0.09–1.89 pmol L^{-1}, n = 605) that crossed the NA within the subtropical gyre from 18°N to 40°N (Bowman et al., 2015), but lower than the range and the unusually high arithmetic mean determined in the South Atlantic along the GEOTRACES-GA10 transect (0.39–3.39 pmol L^{-1}, n = 375; Bratkič, personal communication, and 1.45 ± 0.60 pmol L^{-1}; Bratkič et al., 2016, respectively).

The overall distribution of the HgT_{UNF} concentrations along the GEOTRACES-GA01 transect is represented in Fig. 2. The main feature of HgT_{UNF} concentrations is an eastward increase, from Greenland to Europe, and downward increase, from sub-surface to bottom waters. In addition, lowest and highest (most variable) HgT_{UNF} values were encountered in surface/sub-surface waters, where Hg evasion to the atmosphere and high particulate matter concentrations may generate low and high HgT_{UNF} concentrations, respectively. Out of the 141 filtered samples that were analysed, altogether, the filtered fraction of Hg (HgT_F) represents, on average, 78% (range: 36–98%) of the HgT_{UNF} (Fig. 3). Excluding the upper 100 m, where the biogenic suspended particles are usually abundant, and the stations located on the shelf and slope, where particulate matter from continental sources are usually present, the HgT_F fraction represents, on average, 84 % (range: 72–98%) of the HgT_{UNF}. In addition, in the LS, HgT_F / HgT_{UNF} mean ratios were rather low ranging 62–92 %, with a mean of 76 %. In fact, the primary production was high in spring 2014 in LS, and the winter convection, which reached 1400 m, conveyed surface particles at depth (Yashayaev et al., 2015; Lemaitre et al., this issue). If we exclude the LS from the HgT_F mean computation, we obtain a mean percentage HgT_F / HgT_{UNF} ratio of 91%, which is similar to values (~ 90%) obtained along the GEOTRACES-GA03 zonal and meridional transects (Bowman et

al., 2015). In the following sub-sections, detailed descriptions of the HgT_{UNF} profiles for the five following oceanographic environments are given: LS, IrS, Iceland basin (IcB), Eastern North Atlantic basin (ENAB) and Iberian abyssal plain (IAP).

4.1. Labrador Sea (Stas. 61 to 78)

In the LS, the HgT_{UNF} concentrations ranged from 0.25 to 0.67 pmol L^{-1}, with a mean (± standard deviation) of 0.44 ± 0.10 pmol L^{-1} (n = 113). Distribution, source, and cycling of Hg in the LS have been described and discussed in detail in a companion paper (Cossa et al., 2017b). In summary: highest HgT_{UNF} concentrations were found in the waters of the Labrador Current (LC) receiving freshwaters from the Canadian Arctic Archipelago, and in the waters over the Labrador shelf and continental rise. In the LSW formed during the 2014 winter convection, HgT_{UNF} concentrations were low (0.38 ± 0.05 pmol L^{-1}, n = 23) and increased gradually with depth (up to > 0.5 pmol L^{-1}) in the Northeast Atlantic Deep Waters.

4.2. Irminger Sea (Stas. 40–60)

HgT_{UNF} concentrations in the IrS waters varied from 0.22 to 0.76 pmol L^{-1}, with a mean of 0.45 ± 0.10 pmol L^{-1} (n = 103). In the IrSPMW, which was encountered in the upper1000 m near the East Greenland and the upper 500 m in the rest of the IrS (Fig. 4a in García-Ibáñez et al., this issue), HgT_{UNF} values span between 0.29 and 0.42 pmol L^{-1} (Fig. 2). Deeper, HgT_{UNF} increased up to 0.50 and 0.63 pmol L^{-1} in LSW (~1000 m) and ISOW (~2500 m), respectively. Lower HgT_{UNF} concentrations (0.40–0.50 pmol L^{-1}) were associated with DSOW in the very bottom waters (Sta. 42-44, Fig. 2).

4.3. Iceland Basin (Stas. 34–38)

304 HgT_{UNF} concentrations in the IcB ranged from 0.18 to 0.65 pmol L^{-1}, with a mean of
305 0.46 ± 0.10 pmol L^{-1} (n = 51). In the top 100 m of the water column, HgT_{UNF}
306 concentrations were quite variable (0.25-0.62 pmol L^{-1}) probably as a result of the
307 counteracting importance of Hg evasion to the atmosphere and high particulate matter
308 and/or complexing substance concentrations. West of the IcB (Sta. 38), contrasting
309 HgT_{UNF} levels were found on both sides at 500 m, characterized by a thermohaline
310 gradient (Fig. 2a and b in García-Ibáñez et al., this issue). In the top waters, HgT_{UNF}
311 levels were depleted to 0.18 pmol L^{-1}, whereas, below 500 m, they were much higher
312 and converge to values close to what we found, at the same depths in the adjacent IrS
313 (~0.60 pmol L^{-1}, Sta. 40). In the bottom waters, constituted by more than 50% of ISOW
314 (García-Ibáñez et al., this issue), HgT_{UNF} concentrations reached values > 0.50 pmol L^{-1}.

315 ***4.4. Eastern North Atlantic Basin (Stas. 17–32)***

316 The HgT_{UNF} concentrations in the ENAB varied from 0.18 to 1.14 pmol L^{-1}, with a
317 mean of 0.61 ± 0.18 pmol L^{-1} (n = 174). The ENAB, also named Western European
318 Basin, is characterized by a complex vertical stratification of the water column. The
319 HgT_{UNF} vertical profiles at all the stations of the ENAB were characterized by a
320 complex but reproducible pattern depicting (i) two maxima peaks (the upper at
321 subsurface, the lower within the intermediate waters), and below, (ii) a HgT_{UNF}
322 enhancement starting from 2500 m towards the bottom (Fig. 2). The position and
323 intensity of the peaks vary with longitude. The upper peak, which occurs within the top
324 200 m, is only 0.48 pmol L^{-1} at Sta. 29, but reaches 1.14 pmol L^{-1} at Sta. 19 (Fig. 2).
325 The vertical position of maxima of the lower peak and deepens eastwards, from 200 m
326 down to 800 m, concurrently with an increase of its magnitude (Fig. 2). The position of

the upper peaks suggests a relation with position of the fluorescence maximum (data not shown), whereas the position of the lower peaks, which is close to the maximum of Apparent Oxygen Utilization (AOU) that rose above 70 µmol L^{-1} (Fig. 2), suggests a dependence on the organic matter remineralization (see Discussion below). Between 1400 and 2500 m, in the layer corresponding to LSW, HgT_{UNF} concentrations were quite uniform, with a mean concentration of 0.54 ± 0.04 pmol L^{-1} (n = 18). HgT_{UNF} concentration increased from 3000 m downwards to the sea bottom, consisting of $NEADW_L$, where it reaches 0.95, 0.97, 1.03 and 1.13 pmol L^{-1} at Sta. 21, 19, 25 and 23, respectively.

4.5. Iberian Abyssal Plain (Stas. 1–15)

In the IAP, HgT_{UNF} concentrations ranged from 0.19 to 1.54 pmol L^{-1}, with a mean of 0.69 ± 0.23 pmol L^{-1} (n = 94). The highest HgT_{UNF} concentrations were measured in the upper 100 m near the shelf slope. At Sta. 2, the only station on the European shelf (bottom at 152 m), the HgT_{UNF} concentrations increased from 10 m to the bottom, from 0.38 to 0.86 pmol L^{-1}, but did not differ from the open NA ocean levels. Off-shore, at Sta. 1, 11, 13 and 15 (Fig. 2), the vertical distributions of HgT_{UNF} presented a certain similarity with those of the eastern ENAB, but with an additional third deep peak. As in the eastern ENAB, the upper peak is associated with subsurface waters, and the second, centered around 800 m, is associated with the oxygen minimum of $SPMW_8$. The third peak, centered around 1100-1200 m, is associated with the salinity maximum of the core of MW (Fig. S2). The presence of a HgT_{UNF} peak in the MW was still visible westwards, at Sta. 17, 19 and 23, near 1100 m, as a shoulder of the main peak at 800 m (Fig. 2). Deeper in the water column, HgT_{UNF} increased gradually from 2000 m (LSW)

to 3000 m (ISOW), 3500 m and below ($NEADW_L$), where HgT_{UNF} concentrations reached 0.87 to 1.04 pmol L^{-1} depending on the station.

In summary, the HgT_{UNF} mean concentrations were low and similar in the basins of the Subpolar Gyre (0,44, 0.45 and 0.46 pml L^{-1} for LS, IrS, and IcB respectively), whereas they exceeded 0.60 pml L^{-1} in the Subtropical Gyre (0.61 and 0.69 pml L^{-1} for ENAB and IAP, respectively). On the other hand, the profiles were rather homogenous in the Subpolar Gyre compared to the multipeak vertical distribution observed in the Subpolar Gyre (Fig. 2). A multipeak pattern was also observed in 1994 in the Eastern Atlantic slope water column in the Celtic Sea (Cossa et al., 2004). The shape of the Hg profiles exhibited the same peaks in the same water masses as the ones observed in this study (i.e., SPMW and MW). However, HgT_{UNF} concentration levels, measured 20 years ago, were much higher varying mostly often from 0.3 pmol L^{-1} in sub-surface waters to more than 2.0 pmol L^{-1} at depth.

5. Discussion

5.1. Biogeochemical and hydrographical controls on HgT distribution

Main paths of the Hg cycle in the open ocean can be briefly summarized as follows. Direct atmospheric deposition is the dominant source of Hg for the oceans, most of the deposited Hg is re-emitted in the atmosphere, and a minor Hg fraction is drawn down to the ocean interior with downwards convecting waters or associated with sinking particles. At depth, the dissolution of particulate matter, produced as a result of organic matter microbiological remineralization, remobilizes Hg from particles produced in the

euphotic zone. The biological pumping/regeneration process results in a relationship between Hg concentrations and nutrient or dissolved oxygen concentration (or AOU), which are proxies of the organic matter remineralization (mainly the microbial respiration) that the sample has experienced since it was last in contact with the atmosphere. Such a biogeochemical behaviour, which is qualified of "nutrient-like" behaviour, is observed in the present study (Fig. 4). The correlation coefficient (R) between HgT_F and the AOU, obtained from *in situ* measurements of dissolved oxygen and temperature, reached the highly statistically significant value of 0.87 (n = 141, $p < 0.01$). Similar behaviour was already observed in the water column near the shelf edge of the western European margin (Cossa et al., 2004), and elsewhere in the NA (Lamborg et al., 2014; Bowman et al., 2015). Thus, present results confirm that biological uptake and regenerative processes appear to control a large part of the oceanic Hg distribution in the Subpolar and Subtropical gyres of the NA.

Hydrological circulation may also impact the Hg distribution in the NA. We estimated the HgT_{UNF} (and AOU) values of each SWT using eOMP (Table 1). The correlation coefficient between observed and predicted (eOMP-based) values through Eq. (1) (Material and Methods section) for HgT_{UNF} is 0.71. The estimated HgT_{UNF} concentrations vary significantly between SWTs from 0.32 ± 0.03 to 1.04 ± 0.02 pmol L^{-1}, for the IrSPM to the $NEADW_L$, respectively. However, a large part of the HgT_{UNF} between SWTs is due to the regeneration process as suggested by the correlation coefficient (R = 0.82) of the linear relationship of HgT_{UNF} versus AOU (Fig. 5). Based on this model (HgT_{UNF} = 0.0043*AOU+0.3547), we calculated mean "corrected" HgT_{UNF} concentrations for each identified SWT for a zero AOU concentration.

"Corrected" mean values range from 0.22 to 0.61 pmol L^{-1} in IrSPMW and NEADW, respectively (Table 1). This variation should result from the origin, the route and the age of each SWT. The "corrected" HgT_{UNF} values of IrSPMW-PIM-SPMW-DSOW-LSW, which are formed in the Subpolar gyre and in the NS during the last winter, present very low and similar values 0.22-0.31 (Table 1). Even, the IrSPMW is the youngest SPMW formed in the IrS as a result of air-sea interaction of the waters transported northwards by the NAC (e.g., McCartney and Talley, 1984); the low HgT_{UNF} value found in the IrSPMW may result from a net Hg evasion in this region, consistently with the conclusion that Western and Central NA are a net source of Hg for the atmosphere (Mason et al., 2017). On the contrary, on the Eastern NA side, where Hg deposition and evasion are rather similar (Mason et al., 2017), the ENACW shows higher "corrected" HgT concentration (0.41 pmol L^{-1}, Table 1). The highest "corrected" HgT_{UNF} mean concentration is calculated for $NEADW_L$ (0.61 pmol L^{-1}, Table 1), which is the dominant water mass in the bottom IAP, with its main core below ~3500 m-depth and spreading down to the bottom (see figure 4 in García-Ibáñez et al., this issue). This water mass presents a significant component from Southern Ocean (AABW), which is known to be Hg-rich (HgT_{AABW} = 1.35 ± 0.39 pmol L^{-1}, Cossa et al., 2011). The same rationale can be drawn for the "corrected" HgT_{UNF} concentration in MW (0.41 pmol L^{-1}, Table 1). Indeed, recent measurements in the waters of the Western Mediterranean give HgT_{UNF} values varying between 0.53 and 1.25 pmol L^{-1} within the layer that flows out of the Mediterranean Sea at the Strait of Gibraltar (Cossa and Coquery, 2005; Cossa et al., 2017a).

In summary, the distribution pattern of HgT_{UNF} along the GEOTRACES-GA01 transect, modeled by mixing of SWTs (Fig. S4), stresses the importance of Hg scavenging by plankton and organic matter regeneration, but also show that a part of Hg-enrichment in certain SWTs, among which MW and NEADW, is due to preformed Hg outside the NA. This type of results, characterizing the Hg concentrations in principal oceanic water masses, should contribute to the refinements in model formulation and predictability.

5.2. Change in anthropogenic Hg in LSW

Evidence for a decrease in the Hg anthropization in the NA waters can be obtained from the comparison of the present results with those obtained twenty years ago with similar clean sampling and analytical techniques. In a companion paper (Cossa et al., 2017b), we have already compared the present findings for the convection layer in the LS with the results of the 1993 International Oceanographic Commission cruise (Mason et al., 1998). Between 1993 and 2014 the decrease in HgT_{UNF} concentrations would have been more than a factor of two (1.14 ± 0.36 pmol L^{-1} *versus* 0.40 ± 0.07 pmol L^{-1}). However, bearing in mind the uncertainty of the accuracy of early numbers, this magnitude of the decrease cannot be taken for granted. To circumvent the difficulty, the approach to estimate the anthropogenic Hg (Hg_{Anth}) concentrations in subsurface waters, proposed by Lamborg et al. (2014), can be used. Hg_{Anth} is inferred from the difference between measured HgT_{UNF} concentrations and the concentrations predicted based on a worldwide relationship between deep ocean Hg concentrations and remineralised phosphate (Lamborg et al., 2014), with a Redfield ratio of 141 between AOU and remineralized phosphate (Minster and Boulahdid, 1987) a more representative

value for the NA than the global value of 170 proposed by Anderson and Sarmiento (1994). The LSWs take less than 20 years (Doney et al., 1997) to flow eastward more than 3000 km from the LS eastward to the Subtropical Gyre of the NA. Along its path, LSW bears the record of Hg incorporation at the time of their formation, thus sampling along its flow path allows the observation of decadal variations in anthropogenic Hg inputs to the NA. In the NA, estimation of Hg_{Anth} concentrations in the core of LSW, defined within potential density of 27.74 and 27.82, account for 36 ± 0.07 % of the HgT_{UNF}, and are one third lower for younger waters (LS and IrS: 0.16 ± 0.11 pM) than for older waters (IcB and ENAB: 0.24 ± 0.06 pM) (Fig. 6). This 30%-decrease in Hg concentrations are consistent (i) with the observations of a temporal decrease of Hg in the marine boundary layer of the NA (Sprovieri et al., 2010; Weigelt et al., 2014) over the last two decades, and with (ii) the estimated decline in Hg concentrations in subsurface waters of the NA estimated by models during the last decades (e.g., Soerensen et al., 2012).

This means that LSW formed in the 1990s' in the LS, and currently present in the ENAB, received more Hg_{Anth} from the atmosphere than the $LSW_{2014\text{-}2015}$ "vintage". These results contrast with what can be deduced from the vertical profile of HgT_{UNF} in the LS, where the Hg regeneration in the water column is sufficient to account for the Hg increase between the shallow LSW layer ($LSW_{2014\text{-}15}$) and the deep LSW layer ($LSW_{1987\text{-}94}$) (Cossa et al., 2017b). This discrepancy between these two deductions suggests that LSW, which are present in the Eastern NA, is likely older (and more imprinted by legacy Hg_{Anth}) than the LSW currently present in the LS.

5.3. Latitudinal transport of Hg

463 The transport of HgT_{UNF} per unit of water mass, calculated with Eq. (2) (Material and
464 Methods section), are given in Table 2. We also applied Eq. (2) separately to the upper
465 and lower limbs of the AMOC and computed the transports of HgT_{UNF} per water mass
466 for the two limbs. The velocity fields across the Portugal-Greenland transect was
467 calculated using inverse model constrained by Doppler current profiler velocity
468 measurements (Zunino et al., this issue). The volume transport per SWT was computed
469 by combining this velocity fields with the results of the eOMP (García-Ibáñez et al., this
470 issue).

471 The mean (velocity-weighted) HgT_{UNF} concentration of the water advected
472 northwards within the upper limb of the AMOC is 0.55 pmol L^{-1}, whereas the one
473 advected southwards within the lower limb of the AMOC is 0.40 pmol L^{-1}. Across the
474 Portugal-Greenland transect, there is a northward HgT_{UNF} transport within the upper
475 limb of the AMOC (10.20 mmol s^{-1}), and a southward HgT_{UNF} transport within the
476 lower limb (7.12 mmol s^{-1}), resulting in a net northward transport of 97.2 kmol yr^{-1}.
477 Most of the HgT_{UNF} southward transport is due to IrSPMW and ISOW displacements,
478 whereas HgT_{UNF} northward transport is associated with ENACW and SPMW
479 displacements (Table 2). The Hg exchange across the LS section can be roughly
480 estimated at 133 kmol yr^{-1}, using the mean southward water transport of the shelf edge
481 LC is at the Seal Island transect (Hamilton Bank near Stas. 77 and 78) which is 7.5 Sv,
482 according to Han et al. (2008) and a mean HgT concentration of 0.56 pmol L^{-1} (Cossa et
483 al., 2017b). Thus, from our "snap shot" study, the net Hg exchange across the GEOVIDE
484 transect, which crosses the LS and the NA from Portugal and Greenland, would be an
485 Arctic loss of 36 kmol yr^{-1}. In comparison, Soerensen et al. (2016), based on a mass

balance budget, estimated that "Arctic seawater is enriched in total Hg relative to inflowing waters from the North Atlantic and North Pacific Oceans at all depths resulting in a 26 Mg a^{-1} (i.e., 130 kmol a^{-1}), net loss from the Arctic *via* circulation".

6. Summary and conclusions

HgT_{UNF} concentrations in the waters along the GEOTRACES-GA01 transect, which crossed the NA from 40°N to 60°N (Portugal to Canada), ranged from 0.16 to 1.54 pmol L^{-1}, but with 97 % of the values lower than 1.00 pmol L^{-1} and a geometric mean of 0.51 pmol L^{-1} (n = 535). The dissolved fraction (< 0.45 µm) of HgT, determined on 141 samples, averaged 78 % of the HgT_{UNF} for the entire data set, 84 % for deep open sea waters, and 91 % if the Labrador Sea data, where the primary production was high, are excluded. HgT_{UNF} concentrations increased eastwards and downwards. The HgT_{UNF} concentrations were similarly low in the Subpolar Gyre waters (~ 0.45 pmol L^{-1}), whereas they exceeded 0.60 pmol L^{-1} in the Subtropical Gyre waters, especially within $NEADW_L$. The relationship between HgT_F and AOU, which indicates a nutrient-like behavior for Hg in the NA, attests to the influence of organic matter regeneration on HgT mobilization. The distribution pattern of HgT_{UNF} along the transect, modeled by mixing of SWTs, show Hg-enrichments in MW and NEADW, and low Hg concentrations in younger water masses formed during the last winter at high latitudes. Using the HgT_{UNF} fraction unexplained by regeneration processes as a proxy for Hg_{Anth}, we observed geographical trend in the Hg_{Anth} in the LSW along its eastward journey in the NA, characterized by an eastward increase, which suggests that Hg incorporation in the downwelling waters of the LS has decreased over the last 20 years, in parallel with

509 the decrease of Hg concentrations in the NA troposphere. By combining the velocity
510 fields with the results of the eOMP, a net northward Hg transfer of 97.2 kmol yr^{-1} across
511 the Portugal-Greenland transect can be calculated as a result of the AMOC. Taking into
512 account the southern Hg export with the LC, the net Hg exchange along the entire
513 GEOVIDE transect would be an Arctic loss of 36 kmol yr^{-1}.

514

515 ***Abbreviations***: AABW, Antarctic Bottom Water; AFS, atomic fluorescence
516 spectrometer; AMOC, Atlantic Meridional Oceanic Circulation; AOU, Apparent
517 Oxygen Utilization; CFCs, chlorofluorocarbons; CRM, certified reference material; DL,
518 detection limit; DSOW, Denmark Strait Overflow Water; DWBC, Deep Western
519 Boundary Current; EGC, Eastern Greenland Current; ENAB, Eastern North Atlantic
520 basin; ENACW, East North Atlantic Central Water; eOMP, extended Optimum
521 Multiparameter analysis; Hg, mercury; HgT_{Anth}, anthropogenic HgT; HgT, total
522 mercury; HgT_{UNF}, unfiltered HgT; HgT_{F}, filtered HgT; IAP, Iberian abyssal plain; IcB,
523 Iceland basin; IOC, International Oceanographic Commission; IrS, Irminger Sea;
524 ISOW, Iceland-Scotland Overflow Water; LC, Labrador Current; LS, Labrador Sea;
525 LSW, Labrador Sea Water; MW, Mediterranean Water; NA, North Atlantic Ocean;
526 NAC, North Atlantic Current; NADW, North Atlantic Deep Water; $NEADW_{L}$, Lower
527 North East Atlantic Deep Water ; PIW, Polar Intermediate Water; SPMW, Subpolar
528 Mode Water; SWT, Source Water Type; WGC, Western Greenland Current.

529

530 ***Acknowledgments***: Thanks are due to members of the GEOVIDE team for participating
531 to data acquisition: F. Alonso Pérez, R. Barkhouse, V. Bouvier, P. Branellec, L.
532 Carracedo Segade, M. Castrillejo, L. Contreira, N. Deniault, F. Desprez de Gesincourt,
533 L. Foliot, D. Fonseca Pereira, E. Grossteffan, P. Hamon, C. Jeandel, C. Kermabon, F.
534 Lacan, P. Le Bot, M. Le Goff, A. Lefebvre, S. Leizour, N. Lemaitre, O. Menage, F.
535 Planchon, A. Roukaerts, V. Sanial, R. Sauzède, and Y. Tang. A special thank is also due
536 to the R/V "*Pourquoi Pas?"* crew and Captain G. Ferrand, and the DT INSU (E. de
537 Saint Léger, F. Pérault) who organized the rosette deployment/recovery processes. This
538 research was founded by the French National Research Agency (ANR-13-BS06-0014,
539 ANR-12-PDOC-0025-01), the French National Center for Scientific Research (CNRS-
540 LEFE-CYBER), the LabexMER (ANR-10-LABX-19), the Global Mercury Observation
541 System (GMOS, N°265113 European Union project), and the European Research
542 Council (ERC-2010-StG-20091028). For this work M.I. García-Ibáñez and F.F. Pérez
543 were supported by the Spanish Ministry of Economy and Competitiveness through the
544 BOCATS (CTM2013-41048-P) project co-funded by the Fondo Europeo de Desarrollo
545 Regional 2014-2020 (FEDER).
546
547

548
549
550 **References**

551 Amyot, M., Gill, G. A., and Morel, F. M. M.: Production and loss of dissolved gaseous
552 mercury in coastal seawater. Environ. Sci. Technol., 31, 3606–3611, 1997.

553 Amos, H. M., J. E. Sonke, J. E., Obrist, D., Robins, N., Hagan, N., Horowitz, H. M.,
554 Mason, R. P., Witt, M., Hedgecock, I. M., Corbitt, E. S., and Sunderland, E. M.:
555 Observational and Modeling Constraints on Global Anthropogenic Enrichment of
556 Mercury. Environ. Sci. Technol., 49, 4036-4047, 2015.

557 Anderson, L. A., and Sarmiento, J. L.: Redfield ratios of remineralization determined by
558 nutrient data-analysis. Glob. Biogeochem. Cycles, 8, 65–80, 1994.

559 Bloom, N. S., and Crecelius, E. A.: Determination of mercury in seawater at sub-
560 nanogram per liter levels, Mar. Chem., 14, 49–59, doi:10.1016/0304-4203(83)90069-5,
561 1985.

562 Bowman, K. L., Hammerschmidt, C. R., Lamborg, C. H., and Swarr, G. J.:
563 Mercury in the North Atlantic Ocean: The U.S. GEOTRACES zonal and
564 meridional, Deep Sea Res. Part II, 116, 251–261, doi:10.1016/j.dsr2.2014.07.004,
565 2015.

566 Bowman, K. L., Hammerschmidt, C. R., Lamborg, C. H., Swarr, G. J., and
567 Agather, A. M.: Distribution of mercury species across a zonal section of the
568 eastern tropical South Pacific Ocean (U.S. GEOTRACES GP16), Mar. Chem.,
569 186, 156-166, 2016.

570 Brambilla, E., and Talley, L. D.: Subpolar Mode Water in the northeastern Atlantic: 1.
571 Averaged properties and mean circulation, J. Geophys. Res., Oceans, 113(C4), C04025,
572 doi:10.1029/2006JC004062, 2008.

573 Bratkič, A., Vahčič, M., Kotnik, J., Obu Vazner, K., Begu, E., Woodward, E. M. S., and
574 Horvat, M.: Mercury presence and speciation in the South Atlantic Ocean along the
575 40°S transect, Global Biogeochem. Cycles, 30, 105–119, doi:10.1002/2015GB005275,
576 2016.

Bratkič, A.: Chemistry Department, Vrije Universiteit Brussel, Pleinlaan 2, 1050 Brussels, Belgium. Email: arne.bratkic@vub.ac.be.

Cianca A., Santana, R., Marrero, J. P., Rueda, M. J., and Llina, O.: Modal composition of the central water in the North Atlantic subtropical gyre, Ocean Sci. Discuss., 6, 2487–2506, doi:10.5194/osd-6-2487-2009, 2009.

Cossa, D., and Courau, P.: An international intercomparison exercise for total mercury in seawater, Appl. Organometal. Chem., 4, 49–54, doi:10.1002/aoc.590040109, 1990.

Cossa, D., and Coquery, M.: The Mediterranean mercury anomaly, a geochemical or a biological issue. pp 177-208. In: *The Mediterranean Sea*. Handbook of Environmental Chemistry, Vol 5. Saliot, A. editor. Springer, 413 p. 2005. ISSN 1433-6863, 2005.

Cossa D., Cotté-Krief M.-H., Mason R. P., and Bretaudeau-Sanjuan J.: Total mercury in the water column near the shelf edge of the European continental margin, Mar. Chem., 90, 21–29, doi:10.1016/j.marchem.2004.02.019, 2004.

Cossa, D., Heimbürger, L.-E., Lannuzel, D., Rintoul, S. R., Butler, E. C. V., Bowie, A. R., Averty, B., Watson, R. J., Remenyi, T.: Mercury in the Southern Ocean. Geochim. Cosmochim. Acta, 7, 4037–4052, doi:10.1016/j.gca.2011.05.001, 2011.

Cossa, D., Durrieu de Madron, X., Schäfer, J., Guédron, S., Marusczak, N., Castelle, S., and Naudin, J.-J.: Sources and exchanges of mercury in the waters of the Northwestern Mediterranean margin, Prog. Oceanogr. doi.org/10.1016/j.pocean.2017.05.002, 2017a.

Cossa, D., L.-E. Heimbürger, L.-E., Sonke, J. E., Planquette, H., Lherminier, P., García-Ibáñez, M. I., Pérez, F. F., and Sarthou, G.: Sources, recycling and transfer of mercury in the Labrador Sea (GEOTRACES-GEOVIDE cruise). Mar. Chem., doi.org/10.1016/ j.marchem.2017.11.006, 2017b.

Cutter, G. A., and Bruland, K. W.: Rapid and noncontaminating sampling system for trace elements in global ocean surveys. Limnol. Oceanogr. - Methods 10, 425–436, doi:10.4319/lom.2012.10.425, 2012.

Cutter, G., Casciotti, K., Croot, P., Geibert, W., Heimbürger, L. E., Lohan, M., Planquette, H., and van de Fliert, T.: GEOTRACES cookbook: Sampling and sample-

handling protocols for GEOTRACES cruises. Version 3, edited by the 2017 GEOTRACES Standards and Intercalibration Committee: Version 3.0; August 2017.

Daniault, N., Lherminier, P., and Mercier, H.: Circulation and transport at the southeast tip of Greenland, J. Phys. Oceanogr., 41, 437–457, doi:10.1175/2010JPO4428.1, 2011.

Daniault, N., Mercier, H., Lherminier, P., Sarafanov, A., Falina, A., Zunino, P., Pérez, F. F., Ríos, A. F., Ferron, B., Huck, T., Thierry, V., and Gladyshev, S.: The northern North Atlantic Ocean mean circulation in the early 21st century, Progr. Oceanogr., 146, 142–158, doi:10.1016/j.pocean.2016.06.007, 2016.

de la Paz, M., García-Ibáñez, M. I., Steinfeldt, R., Ríos, A. F., and Pérez F. F.: Ventilation versus biology: What is the controlling mechanism of nitrous oxide distribution in the North Atlantic?, Global Biogeochem. Cycles, 31, 745–760, doi:10.1002/2016GB005507, 2017.

Doney, S. C., Jenkins, W. J., and Bullister, J. L.: A comparison of ocean tracer dating techniques on a meridional section in the eastern North Atlantic. Deep Sea Res. I, 44, 603–626, 1997.

EPA (Environmental Protection Agency, US): Method 1631, Revision E: Mercury in water by oxidation, purge and trap, and cold vapor atomic fluorescence spectrometry. EPA-821-R-02-019, 2002. http://water.epa.gov/scitech/methods/cwa/metals/mercury/index.cfm, 2002.

Fitzgerald, W. F., Lamborg, C. H., and Hammerschmidt, C. R.: Marine biogeochemical cycling of mercury. Chem. Rev., 107, 641-662, 2007.

Fontela, M., García-Ibáñez, M. I., Hansell, D. A., Mercier, H., and Pérez, F. F.: Dissolved Organic Carbon in the North Atlantic Meridional Overturning Circulation, Sci. Rep., 6, 26931, doi:10.1038/srep26931, 2016.

García-Ibáñez, M. I., Pardo, P. C., Carracedo, L. I., Mercier, H., Lherminier, P., Rios, A. F., and Pérez, F. F.: Structure, transports and transformations of the water masses in the Atlantic Subpolar Gyre, Prog. Oceanogr., 135**,** 18–36, doi:10.1016/j.pocean.2015.03.009, 2015.

García-Ibáñez, M. I., Pérez, F. F., Lherminier, P., Zunino, P., and Treguer, P.: Water mass distributions and transports for the 2014 GEOVIDE cruise in the North Atlantic. This issue.

Gill, G. A., and Fitzgerald, W. F.: Mercury sampling of open ocean waters at the picomolar level, Deep Sea Res. Part A, 32, 287–297, doi:10.1016/0198-0149(85)90080-9, 1985.

Gill, G. A., and Fitzgerald, W. F.: Vertical mercury distributions in the oceans, Geochim. Cosmochim. Acta, 53, 1719-1728, 1988.

Gourcuff, C., Lherminier, P., Mercier, H., and Le Traon, P. Y.: Altimetry combined with hydrography for ocean transport estimation, J. Atmos. Oceanogr. Technol., 28, 1324–1337, doi:10.1175/ 2011JTECHO818.1, 2011.

Han, G., Lu, Z. Wang, Z., Helbig, J., Chen, N., and. de Young, B.: Seasonal variability of the Labrador Current and shelf circulation off Newfoundland, J. Geophys. Res., 113, C10013, doi:10.1029/2007JC004376, 2008.

Heimbürger, L.-E., Sonke, J., Cossa, D., Point, D., Lagane, C., Laffont, L., Galfond, B. T., Nicolaus, M., Rabe, B., and Rutgers van der Loeff, M.: Shallow methylmercury production in the marginal sea ice zone of the central Arctic Ocean, Sci. Rep., 5, 10318, doi:10.1038/srep10318, 2015.

Hewitt, C. N.: Instrumental Analysis of Pollutants. Elsevier Applied Science, 1989.

Kuhlbrodt, T., Griesel, A., Montoya, M., Levermann, A., Hofmann, M., and Rahmstorf, S.: On the driving processes of the Atlantic meridional overturning circulation. *Atlantic* 45**,** RG2001, 2007.

Lamborg, C. H., Hammerschmidt, C. R., Gill, G. A., Mason, R. P., and Gichuki, S.: An intercomparison of procedures for the determination of total mercury in seawater and recommendations regarding mercury speciation during GEOTRACES cruises, Limnol. Oceanogr. – Methods, 10, 90–100, doi:10.4319/lom.2012.10.90, 2012.

Lamborg, C. H., Hammerschmidt C. R., Bowman, K. L., Swarr, G. J., Munson, K. M., Ohnemus, D. C., Lam, P. J., Heimbürger, L.-E., Rijkenberg, M. J. A., and Saito, M. A.:

661 A global ocean inventory of anthropogenic mercury based on water column measurements,
662 Nature, 512, 65–68, doi:10.1038/nature13563, 2014.

663 Lemaitre, N., Planquette, H., Planchon, F., Sarthou, G., Jacquet, S., García-Ibáñez, M.
664 I., Gourain, A., Cheize, M., Monin, L., André, L., Laha, P., Terryn, H., and Dehairs, F.:
665 Particulate barium tracing significant mesopelagic carbon remineralisation in the North
666 Atlantic. Biogeosciences Discuss., https://doi.org/10.5194/bg-2017-400, this issue.

667 Lherminier, P., Mercier, H., Gourcuff, C., Álvarez, M. F., Bacon, S., and Kermabon, C.:
668 Transport across the 2002 Greenland-Portugal section and comparison with 1997, J.
669 Geophys. Res., 112(C07003), doi:10.1029/2006JC003716, 2007.

670 Lherminier, P., Mercier, H., Huck, T., Gourcuff, C., Pérez, F. F., Morin, P., Sarafanov,
671 A., and Falina, A.: The Atlantic Meridional Overturning Circulation and the Subpolar
672 Gyre observed at the A25-OVIDE Section in June 2002 and 2004, Deep-Sea Res., I, 57,
673 1374–1391, doi:10.1016/j.dsr.2010.07.009, 2010.

674 McCartney, M. S.: Recirculating components to the deep boundary current of the
675 northern North Atlantic, Prog. Oceanogr., 29, 283–383, doi:10.1016/0079-
676 6611(92)90006-L, 1992.

677 McCartney, M. S., and Talley, L. D.: The subpolar mode water of the North Atlantic
678 Ocean, J. Phys. Oceanogr., 12, 1169–1188, doi:10.1175/1520-0485(1982)
679 012<1169:TSMWOT>2.0.CO;2, 1982.

680 McCartney, M. S., and Talley, L. D.: Warm-to-cold conversion in the northern North
681 Atlantic Ocean, J. Phys. Oceanogr., 14, 922–935, doi:10.1175/1520-
682 0485(1984)014<0922:WTCWCI>2.0.CO;2, 1984.

683 Mason, R. P., and Fitzgerald, W. F.: The distribution and biogeochemical cycling of
684 mercury in the equatorial Pacific Ocean, Deep Sea Res., Part I, 40, 1897–1924, 1993.

685 Mason, R. P., Fitzgerald, W. F. and Morel, F. M. M.: The biogeochemical cycling of
686 elemental mercury: Anthropogenic influences. Geochim. Cosmochim. Acta, 58, 3191–
687 3198, 1994.

688 Mason, R. P., Morel, F. M. M., and Hemond, H. F.: The role of microorganisms in
689 elemental mercury formation in natural waters. Water Air Soil Poll., 80, 775–787, 1995.

690 Mason R. P., Rolfus K. R., and Fitzgerald W. F.: Mercury in the North Atlantic, Mar.
691 Chem., 61, 37–53, doi:10.1016/S0304-4203(98)00006-1, 1998.

692 Mason, R. P., and Sheu, G.-R. : Role of the ocean in the global mercury cycle. Global
693 Biogeochem. Cycles, 16, 1093, doi:10.1029/2001GB001440, 2002.

694 Mason, R. P., Choi, A. L., Fitzgerald, W. F., Hammerschmidt, C. R., Lamborg, C. H.,
695 Soerensen, A.L., and Sunderland, E.M.: Mercury biogeochemical cycling in the ocean
696 and policy implications. Environ. Res. 119, 101–117, 2012.

697 Mason, R. P., Hammerschmidt, C. R., Lamborg, C. H., Bowman, K. L., Swarr, G. J.,
698 and Shelley, R. U. : The air-sea exchange of mercury in the low latitude Pacific and
699 Atlantic Oceans Deep–Sea Research Part I 122 (2017) 17–28,
700 doi.org/10.1016/j.dsr.2017.01.015, 2017.

701 Mercier, H., Lherminier, P., Sarafanov, A., Gaillard, F., Daniault, N., Desbruyères, D.,
702 Falina, A., Ferron, B., Gourcuff, C., Huck, T., and Thierry, V.: Variability of the
703 meridional overturning circulation at the Greenland-Portugal OVIDE section from 1993
704 to 2010, Prog. Oceanogr., 132, 250–261, doi:10.1016/j.pocean.2013.11.001, 2015.

705 Minster, J.-F., and Boulahdid, M.: Redfield ratios along isopycnal surfaces – a
706 complementary study. Deep Sea Res. Part I, 34, 1981-2003, 1987.

707 Munson, K. M., Lamborg, C. H., Swarr, G. J., and Saito, M. A.: Mercury species
708 concentrations and fluxes in the Central Tropical Pacific Ocean, Global Biogeochem.
709 Cycles, 29, 656–676, doi:10.1002/2015GB005120, 2015.

710 Rhein, M., Fisher, J., Smethie, W. M., Smythe-Wright, D., Weiss, R. F., Mertens, C.,
711 Min, D.-H., Fleischmann, U., and Putzka, A.: Labrador Sea water: Pathways, CFC
712 Inventory, and Formation Rates, J. Phys. Oceanogr., 32, 648–665, doi:10.1175/1520-
713 0485(2002)032<0648:LSWPCI>2.0.CO;2, 2002.

714 Soerensen, A. L., Jacob, D. J., Streets, D. G., Witt, M. L. I., Ebinghaus, R., Mason, R.
715 P., Andersson, M., and Sunderland, E. M.: Multi-decadal decline of mercury in the
716 North Atlantic atmosphere explained by changing subsurface seawater concentrations,
717 Geophy. Res. Let., 39, L21810, doi:10.1029/2012GL053736, 2012.

718 Soerensen, A. L., Jacob, D. J., Schartup, A. T., Fisher, J. A., Lehnherr, I., St. Louis, V.
719 L., Heimbürger, L. E., Sonke, J. E., Krabbenhoft, D. P., and Sunderland, E. M.: A mass
720 budget for mercury and methylmercury in the Arctic Ocean, Global Biogeochem.
721 Cycles, 30, doi:10.1002/2015GB005280, 2016.

722 Sprovieri, F., Pirrone, N., Ebinghaus, R., Kock, H., and Dommergue, A.: A review of
723 worldwide atmospheric mercury measurements, Atmos. Chem. Phys., 10, 8245–8265,
724 doi:10.5194/acp-10-8245-2010, 2010.

725 Taylor, J K.: Quality Assurance of Chemical Measurements. Lewis Publishers, 1987.

726 Tsuchiya, M., Talley, L. D., and McCartney, M. S.: An eastern Atlantic section from
727 Iceland southward across the equator, Deep Sea Res. Part A, 39, 1885–1917,
728 doi:10.1016/0198-0149(92)90004-D, 1992.

729 van Aken, H. M., and Becker, G.: Hydrography and through-flow in the northeastern
730 North Atlantic Ocean: the NANSEN project, Progr. Oceanogr. 38, 297–346,
731 doi:10.1016/S0079-6611(97)00005-0, 1996.

732 Weigelt, A., Ebinghaus, R., Manning, A. J., Derwent, R. G., Simmonds, P. G., Spain, T.
733 G., Jennings, S. G., and Slemr, F.: Analysis and Interpretation of 18 years of mercury
734 observations since 1996 at Mace Head, Ireland, Atmos. Environ., 100, 85–93,
735 doi:10.1016/j.atmosenv.2014.10.050, 2014.

736 Yashayaev, I., and Loder, J. W.: Recurrent replenishment of Labrador Sea Water and
737 associated decadal-scale variability, J. Geophys. Res. Oceans, 121, 8095–8114,
738 doi:10.1002/2016JC012046, 2016.

739 Yashayaev, I., Head, E.J.H., Azetsu-Smith, K. Ringuette, M., Wang, Z., Anning, J.,
740 Punshon, S. 2015b. Environmental Conditions in the Labrador Sea during 2014.
741 Northwest Atlantic Fisheries Organization, Scientific Council Meeting (June 2015),
742 Serial N° N6436, NAFO SCR Doc. 15/015. 33 pages.

743 Zhang, Y., Jaeglé, L., and L. A. Thompson, L. A. : Natural biogeochemical cycle of
744 mercury in a global three-dimensional ocean tracer model, Global Biogeochem. Cycles,
745 28, 553–570, doi:10.1002/ 2014GB004814, 2014.

Zunino, P., Lherminier, P., Mercier, H., Daniault, N., García-Ibáñez, M. I., and Pérez, F. F.: The GEOVIDE cruise in May-June 2014 revealed an intense MOC over a cold and fresh subpolar North Atlantic. This issue.

Figure caption

Figure 1. Schematic view of the water circulation in the North Atlantic Ocean adapted from García-Ibáñez et al. (2015) and Daniault et al. (2016). Red lines indicate the circulation in surface, while blue lines indicated circulation at depth. Black lines represent the GEOVIDE cruise transects (GEOTRACES-GA01). Main geographical features, water masses and currents are indicated: Newfoundland (NFL), United Kingdom (U.K.), United States of America (U.S.A.); Denmark Straight Overflow Water (DSOW), Iceland-Scotland Overflow water (ISOW), Labrador Sea Water (LSW), Lower North East Atlantic Deep water ($NEADW_L$), Mediterranean Water (MW), and North Atlantic Deep Water (NADW), Deep Western Boundary Current (DWBC), Eastern Greenland Current (EGC), Labrador Current (LC), North Atlantic Current (NAC), Western Greenland Current (WGC).

Figure 2. Distribution of unfiltered total mercury (HgT_{UNF}) concentrations along the GEOTRACES-GA01 transect. LS: Labrador Sea; IrS: Irminger Sea; IcB: Iceland basin; ENABw: west part of Eastern North Atlantic basin; ENABe: east part of Eastern North Atlantic basin; IAP: Iberian Abyssal Plain.

Figure 3. Mercury concentrations in filtered (HgT_F) *vs* unfiltered (HgT_{UNF}) samples (n = 141) collected along the GEOTRACES-GA01 transect.

Figure 4. Total Hg in filtered samples (HgT_F) *vs* apparent oxygen utilization (AOU) relationship along the GEOTRACES-GA01 transect.

Figure 5. Total Hg in unfiltered samples (HgT_{UNF}) *vs* apparent oxygen utilization (AOU) relationship within the various Source Water Types.

Figure 6. Anthropogenic HgT (HgT_{Anth}) concentration distribution in the core of the Labrador Sea Water (LSW) (S = 34.9, σ_Θ = 27.74–27.82, 1200–2000 m) between the Labrador Sea and the Eastern North Atlantic basin. HgT_{Anth} values were obtained according to the model by Lamborg et al. (2014). Young LSW corresponds to the "2014-vintage" (LSW_{2014}) formed during winter 2013–2014. The insert shows the Hg concentration decrease in the troposphere over the North Atlantic during the last 20 years according to Soerensen et al. (2012).

Tables

Table 1. Total Hg in unfiltered samples (HgT_{UNF}) *vs* apparent oxygen utilization (AOU) concentrations of each source water type (SWT), calculated according to eOMP (Eq. 1) (see also García-Ibáñez et al., this issue). "Corrected" HgT_{UNF} is a theoretical HgT concentration for a AOU concentration equal to zero, using the equation from figure 5. $ENACW_{12}$: East North Atlantic Central Water of 12°C; $SPMW_8$ and $SPMW_7$: Subpolar Mode Waters of the Iceland basin of 7 and 8°C; IrSPMW: Subpolar Mode Water of the Irminger basin; LSW: Labrador Sea Water; MW: Mediterranean Water; ISOW: Iceland-Scotland Overflow Water; $NEADW_L$: lower North East Atlantic Deep Water; DSOW: Denmark Strait Overflow Water; PIW: Polar Intermediate Water; and $SAIW_6$: Subarctic Intermediate Water of 6°C.

SWT	HgT_{UNF} (pmol L^{-1})	AOU (µmol L^{-1})	"Corrected" HgT_{UNF} (pmol L^{-1})
$ENACW_{12}$	0.47 ± 0.01	14 ± 2	0.41
$SPMW_8$	0.73 ± 0.03	105 ± 4	0.28
$SPMW_7$	0.57 ± 0.03	71 ± 3	0.27
IrSPMW	0.32 ± 0.03	23 ± 4	0.22
$SAIW_6$	0.43 ± 0.03	- 16 ± 4	0.50
MW	0.83 ± 0.05	98 ± 5	0.41
LSW	0.46 ± 0.01	35 ± 1	0.31
$NEADW_L$	1.04 ± 0.02	100 ± 2	0.61
PIW	0.53 ± 0.10	72 ± 11	0.22
ISOW	0.62 ± 0.02	57 ± 2	0.38
DSOW	0.44 ± 0.03	30 ± 4	0.31

Table 2. Water and total Hg in unfiltered samples (HgT_{UNF}) transport by the upper and lower limbs of the Atlantic Meridional Overturning Circulation. Positive (negative) transports correspond to northward (southward) flow.

SWT	Entire water column		Upper limb		Lower limb	
	Water transport (Sv)	HgT_{UNF} transport (mmol s^{-1})	Water transport (Sv)	HgT_{UNF} transport (mmol s^{-1})	Water transport (Sv)	HgT_{UNF} transport (mmol s^{-1})
$ENACW_{12}$	9.5	4.52	9.5	4.52	0.0	0.00
$SPMW_8$	4.1	3.02	3.7	2.70	0.4	0.31
$SPMW_7$	3.3	1.86	1.8	1.01	1.5	0.85
IrSPMW	-10.2	-3.23	-0.6	-0.19	-9.6	-3.04
$SAIW_6$	1.0	0.41	2.4	1.04	-1.5	-0.62
MW	0.7	0.60	0.6	0.53	0.1	0.06
LSW	1.9	0.87	1.4	0.86	0.5	0.21
$NEADW_L$	0.3	0.34	0.0	0.00	0.3_3	0.34
PIW	-2.2	-1.18	-0.1	-0.08	-2.1	-1.10
ISOW	-4.9	-3.04	0.0	0.00	-4.9	-3.04
DSOW	-2.5	-1.09	0.0	0.00	-2.5	-1.09
TOTAL	1.1	3.08	18.7	10.2	-17.7	-7.12

798

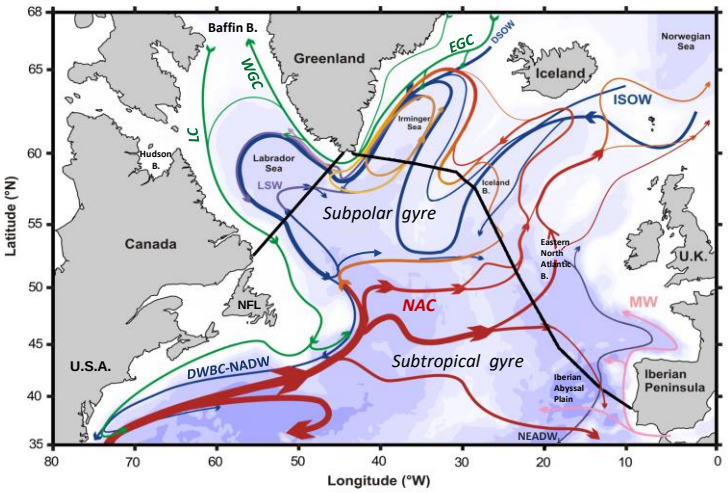

Fig. 1

799

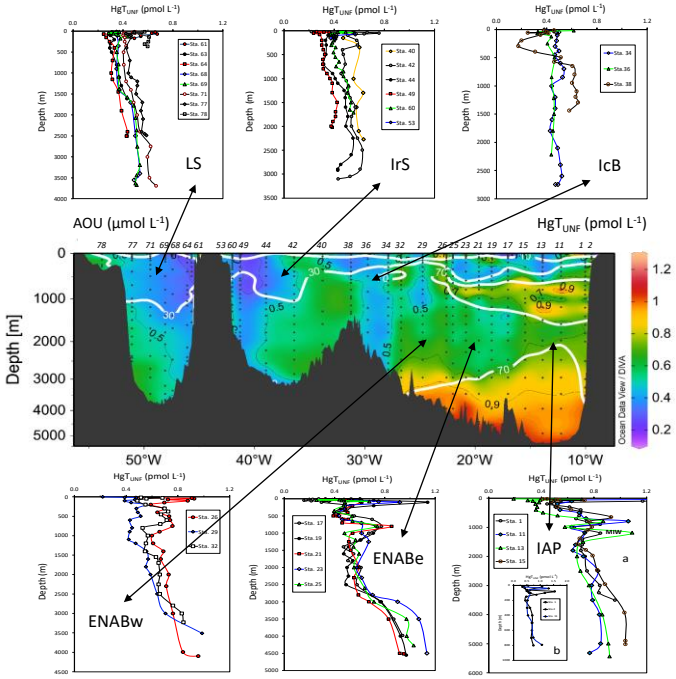

Fig. 2

800

801

802

803

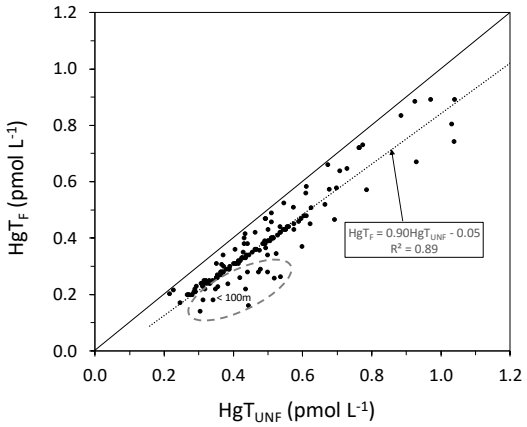

Fig. 3

804

805

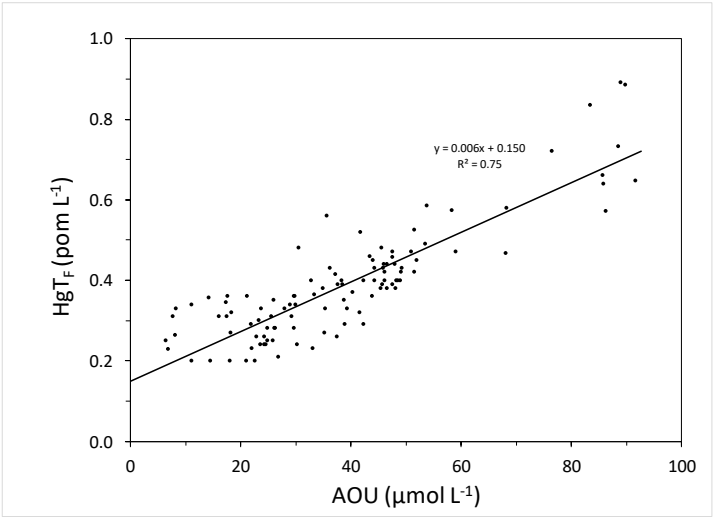

Fig. 4

806

807

808

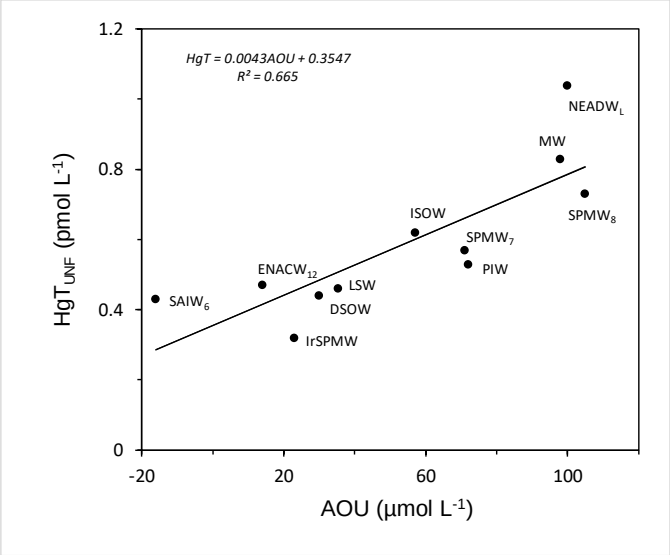

Fig. 5

809

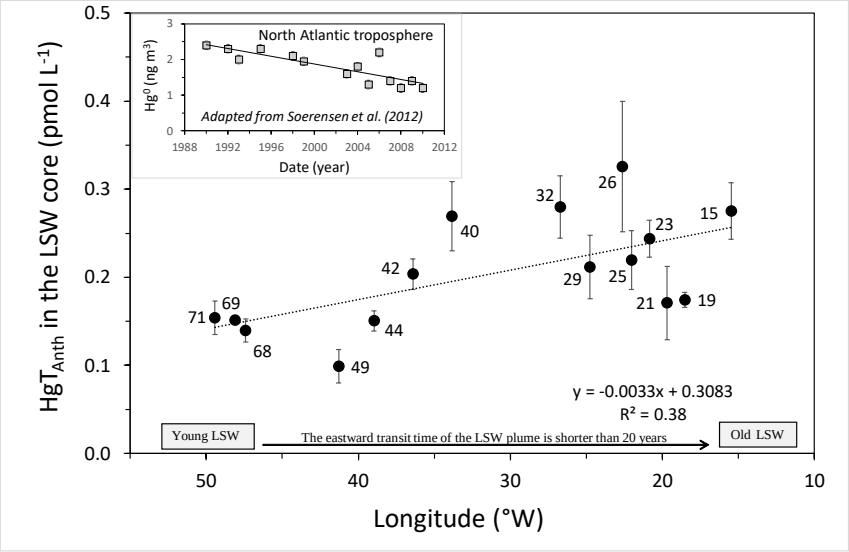

Fig. 6

810

811